In situ measurements of plasma irregularity growth in the cusp ionosphere

K. Oksavik,[1] J. Moen,[2,3] M. Lester,[4] T. A. Bekkeng,[2] and J. K. Bekkeng[2]

Received 16 April 2012; revised 13 August 2012; accepted 17 September 2012; published 1 November 2012.

[1] The Investigation of Cusp Irregularities (ICI-2) sounding rocket was launched on 5 December 2008 from Ny-Ålesund, Svalbard. The high-resolution rocket data are combined with data from an all-sky camera, the EISCAT Svalbard Radar, and the SuperDARN Hankasalmi radar. These data sets are used to characterize the spatial structure of *F* region irregularities in the dayside cusp region. We use the data set to test two key mechanisms for irregularity growth; the Kelvin-Helmholtz (KH) and gradient drift (GD) instabilities. Except for a promising interval of 4–6 km irregularities, the KH growth rate was found to be too slow to explain the observed plasma irregularities. The time history of the plasma gives further support that structured particle precipitation could be an important source of kilometer- to hectometer-scale "seed" irregularities, which are then efficiently broken down into decameter-scale irregularities by the GD mechanism.

Citation: Oksavik, K., J. Moen, M. Lester, T. A. Bekkeng, and J. K. Bekkeng (2012), In situ measurements of plasma irregularity growth in the cusp ionosphere, *J. Geophys. Res.*, *117*, A11301, doi:10.1029/2012JA017835.

1. Introduction

[2] It has been known for more than 50 years that electron density irregularities are a common phenomenon in the *F* region arctic ionosphere [e.g., *Bates*, 1959; *Weaver*, 1965; *Dyson*, 1969]. The spatial scale of individual irregularities can range from tens of km to meters [*Basu et al.*, 1990], and the irregularities are frozen into and drift with the ambient plasma [e.g., *Hanuise et al.*, 1985; *Baker et al.*, 1983]. The irregularities may cause significant negative effects for various radio systems, including ground-to-satellite links and other navigation and communication systems [e.g., *Basu et al.*, 1990, 1998]. Radio waves propagating through these irregularities will experience strong scintillation, both amplitude fading and phase fluctuations up to GHz frequencies [*Basu et al.*, 1988]. These disrupt VHF, UHF and GPS navigation systems at L-band frequencies. At longer wavelengths the plasma irregularities also backscatter radio waves, e.g., at HF frequencies [*Hanuise et al.*, 1981; *Villain et al.*, 1986]. These irregularities are highly field aligned, and a radar beam must be perpendicular to the magnetic field in the *F* region in order to receive significant backscatter [*Bates and Albee*, 1970].

[3] When the interplanetary magnetic field (IMF) is southward these irregularities are closely related to electron density enhancements in high-latitude *F* region called polar cap patches [e.g., *Crowley*, 1996]. Polar cap patches typically have a density which is 2–20 times larger than the surrounding background electron density [*Buchau et al.*, 1983; *Weber et al.*, 1984; *Crowley et al.*, 2000], and polar cap patches can be 100–1000 km wide in the horizontal direction [*Weber et al.*, 1984]. The electron temperature inside a patch is often low and unstructured, indicating no precipitation of auroral electrons when it is located in the polar cap [*Rodger et al.*, 1994]. Patches can be observed both in winter and summer, but are most prominent during moderately disturbed conditions (Kp > 4) [*Weber et al.*, 1984] and near the maximum of the sunspot cycle [e.g., *Dandekar*, 2002; *McEwen et al.*, 2004]. Polar cap patches tend to maximize near equinox and around magnetic noon [*Rodger and Graham*, 1996] and have been observed to drift across the central polar cap [*McEwen and Harris*, 1995; *McEwen et al.*, 1995] and exit the polar cap at night [*Lorentzen et al.*, 2004; *Pryse et al.*, 2006; *Moen et al.*, 2007; *Wood et al.*, 2009]. Irregularities have been observed to populate the entire patch structure, but there is a clear tendency of the strongest irregularities being observed near the trailing edges of patches [*Weber et al.*, 1984].

[4] In literature a long list of mechanisms have been proposed to produce irregularities [*Hanuise et al.*, 1981]; including electrostatic turbulence [*Kelley and Kintner*, 1978], low-energy precipitation [*Kelley et al.*, 1980], and plasma instabilities like the electrostatic ion cyclotron instability [*D'Angelo and Motley*, 1962], the E × B gradient drift instability [*Reid*, 1968], the ion-acoustic instability [*Kindel and Kennel*, 1971], the temperature gradient instability [*Hudson and Kelley*, 1976], and the current-convective instability [*Ossakow and Chaturvedi*, 1979]. Several papers

[1]Department of Physics and Technology, University of Bergen, Bergen, Norway.
[2]Department of Physics, University of Oslo, Oslo, Norway.
[3]University Centre in Svalbard, Longyearbyen, Norway.
[4]Department of Physics and Astronomy, University of Leicester, Leicester, UK.

Corresponding author: K. Oksavik, Department of Physics and Technology, University of Bergen, PB 7803, NO-5020 Bergen, Norway. (kjellmar.oksavik@ift.uib.no)

0148-0227/12/2012JA017835

have provided detailed reviews of the various mechanisms [e.g., *Fejer and Kelley*, 1980; *Hanuise*, 1983; *Tsunoda*, 1988].

[5] At present two fundamentally different mechanisms are thought to dominate the production *F* region irregularities at high latitudes [*Carlson et al.*, 2007]; the Kelvin-Helmholtz (KH) instability, and the E × B gradient drift (GD) plasma instability. The KH plasma instability [*Kintner and D'Angelo*, 1977; *Keskinen et al.*, 1988; *Carlson et al.*, 2007, 2008] is believed to occur if there are severe velocity shears transverse to the magnetic field [e.g., *Oksavik et al.*, 2011]; i.e., the velocity gradient is the source of the free energy. The GD instability [*Reid*, 1968] operates in plasma with a preexisting density gradient and different electron and ion drifts perpendicular to this gradient [*Fejer and Kelley*, 1980]. A polarization electric field is created, and if the resulting polarization E × B drift is of the correct sign the plasma will become unstable, perturbations will amplify, and GD irregularities will break down to smaller scales [e.g., *Keskinen and Ossakow*, 1983]. The GD instability grows when the E × B drift is parallel with a preexisting density gradient, and it is stable to irregularity growth when the E × B drift is anti-parallel with the density gradient [e.g., *Tsunoda*, 1988]. The GD instability has also been extended to include effects like high-latitude currents. The GD mechanism has often been regarded as the dominant mode for the production of *F* region irregularities in the cusp inflow region [*Ossakow and Chaturvedi*, 1979; *Keskinen and Ossakow*, 1983; *Cerisier et al.*, 1985; *Tsunoda*, 1988; *Basu et al.*, 1994; *Gondarenko and Guzdar*, 2004]. Observations [e.g., *Weber et al.*, 1984; *Moen et al.*, 2012] showing a clear tendency for the strongest irregularities being observed near the trailing edges of patches and plasma density enhancements (i.e., in the area where the E × B drift and density gradient are expected to be parallel) have also been interpreted as supporting evidence for the GD mechanism.

[6] Work still remains to be done on the quantification of the KH and GD growth rates. *Moen et al.* [2002] attempted to estimate GD growth rates based on electron density gradients derived from ionospheric topographic images and SuperDARN plasma flow measurements. However, the growth rate they found was too slow to explain the close collocation of the equatorward cusp auroral boundary and the equatorward cusp HF radar backscatter boundary. *Carlson et al.* [2007, 2008] realized that both mechanisms (KH and GD) in principle could act together to produce a more efficient growth of irregularities. They documented a series of quickly developing plasma irregularities observed by scintillation in connection with patch formation over Svalbard and concluded that the onset was too rapid to be explained by any mechanism other than KH. *Carlson et al.* [2007, 2008] therefore suggested that irregularities can be formed in a two-step process, where KH forms the larger-scale "seed" irregularities on which GD later can operate and break the irregularities down to smaller scales. However, this mechanism still needs to be experimentally verified and quantified.

[7] In this paper we will study the growth rates of the KH and GD irregularities in more detail, using high-resolution in situ data of electric fields and plasma density from the Investigation of Cusp Irregularities (ICI-2) sounding rocket together with data from an all-sky camera, EISCAT and SuperDARN. The current paper is part of a series of papers based on ICI-2 rocket data. *Lorentzen et al.* [2010] made a detailed survey of the solar wind conditions and the ionospheric response around the time of the ICI-2 rocket flight, and they studied the formation of a polar cap patch event that was intersected by the rocket payload. *Moen et al.* [2012] presented a more detailed description of the rocket payload, including the first in situ example of electron density structures at decameter scale, and they reported steep kilometer-scale gradients onto which the GD process can efficiently operate. In the current paper we will (1) investigate the spatial structure of the ionospheric irregularities, (2) derive GD and KH growth rates at various spatial scales, and (3) determine which mechanism was dominant in the production of the ionospheric irregularities.

2. Data Presentation

[8] The ICI-2 sounding rocket was launched at 10:35:10 UT on 5 December 2008 from Ny-Ålesund, Svalbard (NYA: 78.9°N, 11.9°E; 76.4° MLAT, 110.2° MLON) to investigate the production of decameter-scale irregularities in the cusp ionosphere associated with HF radar backscatter [*Moen et al.*, 2012]. The solar elevation angle near the rocket apogee was approximately −10° [*Lorentzen et al.*, 2010], and rocket measurements were made between 73.3 and 76.0° MLAT and 13.0–13.6 MLT, see Figure 1. A detailed overview of the solar wind conditions has been provided by Lorentzen et al., and we encourage the interested reader to take a look at Figure 2 of Lorentzen et al. The solar wind speed was 400 km/s. The interplanetary magnetic field (IMF) Bz component was steady and negative (around −6 nT), By was steady and positive (around 4–5 nT), Bx fluctuated around 0 nT and reached a maximum of 4 nT near launch. There were no solar wind density data around launch, but at 11 UT it was around 5 cm^{-3}. For more details, see the work of Lorentzen et al.

[9] Figure 1 summarizes the auroral activity and HF radar measurements. Figure 1a shows an image at 10:37:31 UT of the 630 nm aurora from the UiO/UNIS all-sky camera in Longyearbyen, and Figure 1c shows simultaneous HF backscatter power data from the SuperDARN Finland radar. The all-sky image has been projected onto a magnetic grid, using an assumed emission height of 220 km, and the intensity is shown in color. We notice that the cusp aurora is colocated with high HF backscatter power, in a wide area to the south of Svalbard. In both Figures 1a and 1c, we have indicated the location of the ESR field-aligned 42 m beam with a pink dot, and the ESR 32 m beam with four purple dots, corresponding to locations where the radar beam intersected 100, 200, 300 and 400 km altitude. The ICI-2 trajectory is indicated with a thick black line, and it intersects the ESR 32 m beam from 10:41:15–11:41:34 UT (365–384 s after launch). We notice that ICI-2 was launched in the polar cap, and flew southwest toward the cusp aurora.

[10] To study the formation of irregularities in a plasma that is moving relative to the rocket payload, it is important to know more about the time history of auroral activity and HF backscatter power for individual magnetic flux tubes in the ionosphere. We have therefore used the SuperDARN convection data and the technique of *Oksavik et al.* [2010] to trace backward and forward in time the plasma that

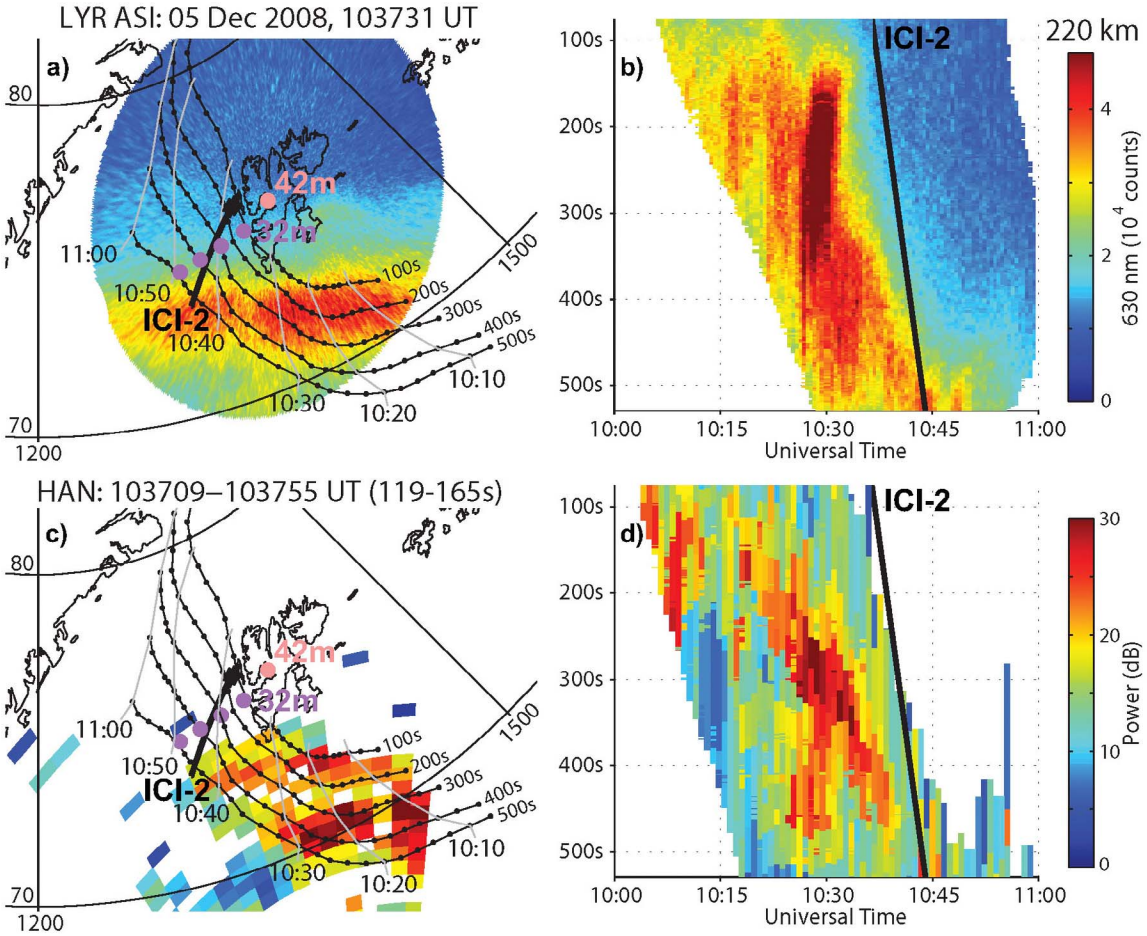

Figure 1. Summary of auroral activity and HF radar measurements during the ICI-2 flight: (a) an image at 10:37:31 UT of the 630 nm aurora from the UiO/UNIS all-sky camera in Longyearbyen projected to 220 km altitude in a magnetic grid, (c) simultaneous HF backscatter power data from the SuperDARN Finland radar, and time history of (b) auroral activity and (d) HF backscatter power for all field lines that drifted across the black ICI-2 track. See text for more details.

intersected the ICI-2 trajectory. The resulting tracks of individual plasma parcels are overlaid in Figures 1a and 1c as black lines. There is one track intersecting the rocket trajectory every 100 s after launch, and tiny black dots every two minutes indicate the time history of each plasma streamline. Universal time is also indicated with light gray guide lines every 10 min. To guide the eye, please look at the 200 s streamline; it originated in the postnoon sector near 70 MLAT and 14.5 MLT, moved through the dayside aurora from 1006 to 1034 UT, intersected the ICI-2 track around 1038 UT, and was near the northeast coast of Greenland around 1100 UT. In a similar way it is seen that all plasma crossing the ICI-2 trajectory originated at lower latitudes in the dusk sector, consistent with stable IMF By positive and Bz negative conditions.

[11] Figures 1b and 1d show the time history of auroral activity and HF backscatter power for all field lines that drifted across the ICI-2 track (which is shown in black). To read this plot, first pick a time of flight along the vertical axis, and then look at a horizontal slice to see the time history of the field line that crossed the ICI-2 track at that particular time. To the left hand side of the ICI-2 track in the

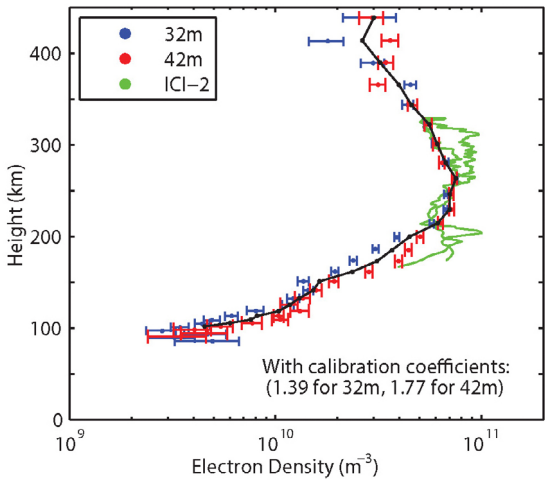

Figure 2. Comparison of electron density profiles from the two ESR beams (32 m in blue, and 42 m in red, and the average of the two in black) with observations from the up and downleg of ICI-2 (in green).

figure is the history of the field line before it reached the ICI-2 track, and to the right hand side is what happened after. We immediately note the following: (1) On their way toward the ICI-2 track the flux tubes traversed an area of intense auroral activity and enhanced HF backscatter power; (2) the aurora and HF backscatter power was for the most part colocated, i.e., a typical signature of the cusp; (3) except for the last 100 s of flight, where the rocket actually intersected aurora, ICI-2 was located 2–3 min drift time poleward of the cusp aurora and the enhanced HF backscatter power, i.e., the irregularities seen by ICI-2 had drifted poleward and the drift time was longer in the early part of the flight; (4) around 10:30 UT there was a transient brightening of the aurora, and flux tubes from this activity intersected the rocket track less than two minutes later, corresponding to 125–140 s after the ICI-2 launch.

[12] Figure 2 compares electron density profiles from the two ESR beams (32 m in blue, and 42 m in red) with observations from the up and downleg of ICI-2 (in green). The ESR data have been integrated for the entire duration of the ICI-2 flight (10 min) in order to look at the average vertical profile of the electron density. By averaging the data in this way we will not be able to reveal any transient variability in the electron density. Around 130 s flight time there was one event passing the ESR that looks very much like a polar cap patch; we refer the interested reader to *Lorentzen et al.* [2010, Figure 4] for more details. But the electron density of that event was just less than two times the background, e.g., slightly smaller than the definition [*Buchau et al.*, 1983; *Weber et al.*, 1984; *Crowley et al.*, 2000]. Because traditional incoherent scatter radar measurements do not measure the absolute electron density, and to have the ESR data match the ICI-2 data at the 263 km altitude *F* region peak, the 32 m and 42 m profiles have been multiplied with calibration coefficients of 1.39 and 1.77, respectively. Still it is noticeable that ICI-2 is observing much finer structures than ESR, which is possible because of the significantly higher temporal and spatial resolution of the rocket measurements compared to the ESR measurements. In the *F* region ICI-2 was making 5700 measurements per second at meter resolution, while the ESR data were averaged over 10 min, several km in the horizontal direction, and 20–30 km in the vertical direction. The finer structure ICI-2 signatures are associated with kilometer to decameter-scale ionospheric irregularities, which we will focus on in the remainder of this paper.

[13] Figure 3a presents electron density measurements from the 4-needle ICI-2 Langmuir probe [*Jacobsen et al.*, 2010; *Bekkeng et al.*, 2010] versus time of flight. In Figure 3b the electron density measurements have been combined with the average electron density profile (shown in Figure 2 as a black line) to produce a graphical representation in color of the vertical electron density distribution along the ICI-2 track (which is shown in black in Figure 3b). To produce Figure 3b we determined the ratio between the average profile and an individual rocket observation (at the altitude of the rocket observation), multiplied the average profile with this number, and repeated the procedure to produce a series of vertical profiles for the duration of the rocket data. From Figure 3b we see that on the upleg ICI-2 intersected the bottom of an intense *F* region (around 140 s), in the middle of the flight ICI-2 was above the *F* peak, and on the downleg ICI-2 flew under a new and intense *F* region associated with the cusp aurora. Figure 3c shows horizontal plasma drift velocities from the ICI-2 electric field instrument (spin-averaged data). The poleward flow (blue) stayed between 1.0 and 1.9 km/s throughout the flight. The westward flow (red) increased from −0.6 to almost 2.0 km/s, and the along-track flow (black) went from −1.2 to −0.3 km/s, as the rocket approached the cusp aurora. In other words, toward the end of the flight the plasma flow was mostly perpendicular to the rocket trajectory, i.e., northwestward.

[14] We can now go one step further and identify spatial structures in the data. The rocket payload is traversing a medium of variable plasma flow, so the horizontal separation Δx between two data samples in the plasma frame of reference is

$$\Delta x = \Delta t \cdot [V_r + V_{E\times B}]. \quad (1)$$

Here Δt is the time between data samples, V_r is the horizontal speed of the rocket payload (around 1 km/s), and V_{ExB} is the component of the E × B plasma drift along the rocket track.

[15] In Figure 3d this technique is used to carry out a spectral analysis of spatial structures in the electron density. Using equation (1), the 5.7 kHz sample rate electron density data in Figure 3a were placed in a horizontal grid. The data were then reduced to 1 m resolution, and a 1024-point Hamming window spectral analysis was carried out. The resulting power spectral density (PSD) is shown in color in Figure 3d versus spatial distance and time after launch. Throughout the flight there were several instances where electron density irregularities extended all the way down to decameter scale. The most prominent example is 125–140 s after launch, when the rocket in 200 km altitude was near an enhancement of the aurora two minutes earlier (cf. Figures 1a and 1c). At this time strong plasma irregularities were seen at all spatial scales from a few hundred meters to less than 10 m. Throughout the flight there were several instances where irregularities extended down to 20–30 m; e.g., around 245–270 s, around 320 s, and 400–450 s after launch.

[16] The same type of spectral analysis can also be performed for the plasma drift data. Using a 32768 point Hamming window, in Figure 3g we show the resulting PSD in color versus spatial distance and seconds after launch. This analysis shows that, contrary to the electron density that had spatial structures all the way down to decameter scale, the drift velocity had almost no fine structures at spatial scales less than 2–3 km. The strongest fluctuations in the drift velocity were seen around 200–230 s. These fluctuations had significant wave power in the 3–10 km range.

[17] This information can also be used to estimate the production of plasma instabilities. For the GD growth rate literature offers two different equations [e.g., *Linson and Workman*, 1970; *Ossakow et al.*, 1978; *Sojka et al.*, 1998]. In a collisional plasma ($4\gamma_{GD} \ll \nu_{\text{in}}$) the linear GD growth rate is

$$\gamma_{\text{GD}} = \frac{V_0 \Delta N}{N_0 \Delta x}. \quad (2)$$

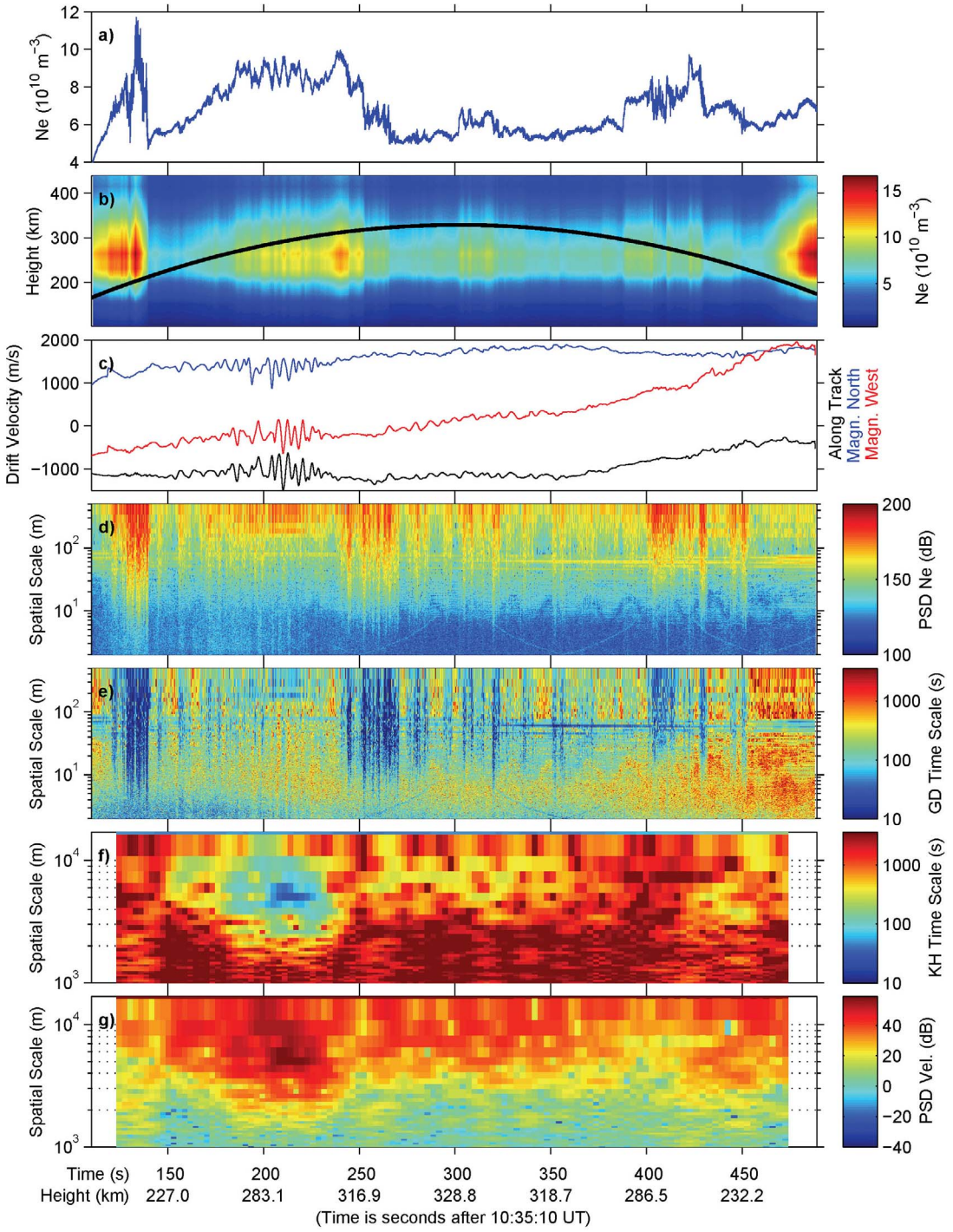

Figure 3. A survey of the ICI-2 electron density and electric field data: (a) electron density measurements from the 4-needle ICI-2 Langmuir probe versus time of flight, (b) a graphical representation in color of the vertical electron density distribution along the ICI-2 track, (c) horizontal plasma drift velocities from the ICI-2 electric field instrument, (d) a spectral analysis of spatial structures in the electron density, (e) the time scale for GD instability growth at various spatial scales versus time, (f) the time scale for KH instability growth at various spatial scales versus time, and (g) a spectral analysis of spatial structures in the electric field. The altitude of the rocket payload is shown both as text along the time axis and as a black line in Figure 3b.

In a collisionless or "inertial" plasma ($4\gamma_{GD} \gg \nu_{in}$) the linear GD growth rate is

$$\gamma_{GD} = \sqrt{\nu_{in}\left(\frac{V_0 \Delta N}{N_0 \Delta x}\right)}. \quad (3)$$

Here ν_{in} is the ion-neutral collision frequency, N_0 is the background density, and $\Delta N/\Delta x$ is the horizontal electron density gradient. Equation (1) gives Δx, and we can use ICI-2 Langmuir probe data for the electron density. V_0 is the plasma drift relative to the neutral atmosphere in the direction parallel to the density gradient (also called the "slip" velocity [*Tsunoda*, 1988]). Unfortunately we have no measurement of the neutral wind at the time, so we will have to assume like *Moen et al.* [2002, 2012] that the neutral wind is negligible compared to the plasma drift velocity, i.e., $V_0 = V_{ExB}$, which is obtained by SuperDARN. *Heelis et al.* [2002] have documented that the neutral wind speed in the *F* region polar cap may reach 60% of the ion drift speed during extended intervals of southward IMF. However, a neutral wind speed which is 60% of the ion drift speed, will only reduce the GD growth rate by a factor of 0.40 in the collisional case (equation (2)), and a factor of 0.63 in the collisionless case (equation (3)).

[18] The KH growth rate can be estimated from work by *Keskinen et al.* [1988]. For ionospheric application the maximized KH linear growth rate is proportional to the velocity gradient, expressed in terms of a velocity difference ΔV and a velocity difference scale length L [*Carlson et al.*, 2008]:

$$\gamma_{KH} = 0.2\Delta V/L. \quad (4)$$

We can now calculate growth or risetimes for the two types of irregularities in the direction along the rocket trajectory (for the direction perpendicular to the rocket track we have no information). In the following we will also ignore loss mechanisms (e.g., diffusion and recombination) and focus only on the production terms. The time scale for irregularity growth is given as $\tau = 1/\gamma$, and in Figure 3e we have plotted the time scale for GD irregularity growth $\tau_{GD} = 1/\gamma_{GD}$ (in logarithmic color scale) at various spatial scales versus time. We notice that 125–140 s after launch there is very efficient growth of GD instabilities at all spatial scales down to a few meters. The efficient growth of GD instabilities was seen when the weak polar cap patch event [*Lorentzen et al.*, 2010] intersected the ICI-2 trajectory. At all scale lengths greater than 10 m, the time scale is just a few seconds (or a few tens of seconds) when we ignore the neutral wind. Assuming a neutral wind speed which is 60% of the ion drift speed only increases the time scale for GD irregularity growth by a factor of 2.50 in the collisional case (equation (2)), and a factor of 1.58 in the collisionless case (equation (3)). We can therefore conclude that the GD mechanism, in a few tens of seconds, will efficiently create a quick cascade of larger scale irregularities to very small spatial scales. The rocket intersected this event only two minutes after a significant enhancement in the aurora (cf. Figures 1a and 1b), so it is possible that structured ionization due to auroral precipitation was essential to create the larger-scale seed ionization that the GD instability builds on, consistent with ideas suggested by *Kelley et al.* [1982] and *Moen et al.* [2002]. There is also efficient growth of GD irregularities at 245–270 s, down to a few tens of meters. The growth of GD irregularities appears to be much slower around 320 s and 400–450 s, but it does not mean that GD irregularities were unable to form. Knowing that the plasma drift was primarily perpendicular to the rocket track, it is possible that GD irregularities could grow in the direction perpendicular to the rocket track.

[19] In Figure 3f we have plotted the time scale for KH irregularity growth $\tau_{KH} = 1/\gamma_{KH}$ (in logarithmic color scale) at various spatial scales versus time. With time scales much longer than 1 h, we notice that the KH instability appears to have been inactive, especially at spatial scales less than a few kilometers. Only around 200–230 s was there a brief interval of 4–6 km KH irregularities with growth time scales down to 30 s (i.e., the KH instability could be active). However, this enhanced growth of KH irregularities was not coincident with any simultaneous growth of GD irregularities.

3. Discussion

[20] It is well known that the cusp ionosphere is an efficient target for coherent HF radio waves, i.e., that the region is composed of decameter-scale field-aligned electron density irregularities with a spatial Fourier component satisfying the Bragg condition [e.g., *Milan et al.*, 1998]. There have also been several papers discussing the colocation of aurora, HF backscatter and particle precipitation in the cusp region. *Rodger et al.* [1995] reported that the equatorward edge of the ionospheric footprint of the optical cusp and the HF radar cusp are colocated to better than 1° in latitude. This result has later been confirmed by other studies [*Milan et al.*, 1999; *Moen et al.*, 2000, 2002]. *Yeoman et al.* [1997] found a colocation of radar backscatter, cusp particle precipitation and optical signatures. *Hosokawa et al.* [2004] documented that high-frequency (0.2–5 Hz) magnetic field fluctuations occur simultaneously with wide HF radar spectra. *Oksavik et al.* [2004] found a near collocation of the equatorward edge of electric field irregularities imposed on the ionosphere and the formation of cusp backscatter irregularities. Their argument was that the strong electric field turbulence will give rise to flow shear (KH) instability and plasma irregularities, as proposed by *Baker et al.* [1995]. This has also been further supported by *Oksavik et al.* [2011], who presented several reversed flow channels that were associated with enhanced SuperDARN backscatter power, all in favor of the KH mechanism.

[21] The current paper presents an example where the KH mechanism can be questioned as a candidate mechanism for decameter irregularity growth at spatial scales less than a few kilometers. KH irregularities were only seen in the km range for a brief interval around 200–230 s, with growth time scales down to 30 s for 4–6 km irregularities. It is also interesting to point out that other reports on KH irregularities [e.g., *Carlson et al.*, 2007, 2008; *Oksavik et al.*, 2011] have all been looking at velocity gradients $\Delta V/L$ in the tens of kilometer range, constrained by the size of individual SuperDARN range gates. The current study is the first search at smaller scales. The fact that no significant velocity gradients were observed at the smallest scales suggests that the KH mechanism is probably most common at spatial scales greater than a few kilometers. *Carlson et al.* [2007,

2008] also argued that the KH mechanism is likely to generate the large "seed" irregularities that the GD mechanism later will build on. However, in the short time interval when the KH instability was active in the several km range, there was no coincident and enhanced growth of GD instabilities at smaller spatial scales. For this reason we did not find any evidence of the two-step mechanism of *Carlson et al.* [2007, 2008]. However, this lack of confirmation does not mean that the *Carlson et al.* [2007, 2008] mechanism is not operational at other times. The flow shears seen by ICI-2 were rather small, and the *Carlson et al.* [2007, 2008] mechanism would also be more efficient in a situation of larger flow shears.

[22] Prior to ICI-2 there were very few studies of the internal substructure of plasma irregularities. *Kelley et al.* [1982] showed data of spatial structures from a Greenland rocket flight, but their data set was not of meter resolution. *Pedersen et al.* [2000] used incoherent scatter radar measurements, which cannot reveal the meter resolution structures that ICI-2 detected. In the current paper we document the spatial structure of irregularities throughout the entire rocket flight. The current data set offers an unprecedented view of kilometer- to meter-scale plasma irregularities in the *F* region cusp ionosphere. Figure 3d reveals that the irregularities were highly variable along a several hundred kilometer horizontal slice. Around 125–140 s after launch the irregularities were seen to extend from a few hundred meters and down to less than 10 m. But there were also intervals of no irregularities at spatial scales less than 100 m, or only very weak irregularities. The latter could explain why SuperDARN sometimes does not observe any backscatter echoes; i.e., significant irregularities may not be present all the time and everywhere when the plasma is stable to irregularity growth.

[23] The current data set provides compelling evidence that the GD instability is a dominant mechanism for irregularity growth in the dayside cusp region. *Moen et al.* [2002] made an initial attempt at quantifying the GD growth rate based on density gradient data from ionospheric tomography in association with 630 nm cusp aurora and a well defined edge of HF radar cusp backscatter. They found a linear growth rate for the GD instability of 12 min. But the tomographic technique requires observations to be made for a range of raypath geometries over a period of several minutes, and *Moen et al.* [2002] pointed out that the resultant integration effect in a poleward convecting flow will smooth out the density gradient to some degree, so their time scale for irregularity growth could be an overestimate by possibly up to an order of magnitude. They concluded that a time scale of the order of minutes would be needed for the irregularities to develop, during which time the prevailing convection would have carried the ionization poleward by a distance greater than the spatial resolution of the measurements ($\sim$25 km). Hence, a clear spatial separation would be expected between the backscatter boundary and the boundary of the cusp auroral emissions. No such division was observed, and *Moen et al.* [2002] concluded that the operation of the GD mechanism on the observed meso-scale gradient was inadequate to explain the observations. With high-resolution data from a subset of the ICI-2 flight, *Moen et al.* [2012] found the first evidence of GD time scales that were 15–70 times faster than the initial estimate of *Moen et al.* [2002]. The study of *Moen et al.* [2012] focused on a 2 s interval in the later part of the ICI-2 flight (from 427.5 to 431.0 s flight time), where kilometer-scale density gradients ascribed to electron precipitation gave a GD time scale of 47.6 s in the direction along the rocket track.

[24] In the current paper we have made a more thorough analysis of the complete ICI-2 data set. We found the most efficient irregularity growth 125–140 s after launch; only two minutes after a significant enhancement in the aurora, cf. Figure 1c. It also points at soft particle precipitation as a likely contributor to irregularity growth. *Oksavik et al.* [2004] point out that the colocation in latitude of the onset of small-scale irregularities responsible for backscatter and the optical emissions is most easily explained if both have a common source. Backscattering of radar signals arises from irregularities transverse to the magnetic field at the Bragg scale, which is about 10–20 m for typical SuperDARN observations. Red-line 630 nm cusp aurora arises from precipitation of low-energy magnetosheath particles that also cause enhancements in electron density at *F* region altitudes. *Walker et al.* [1999] suggested that soft precipitation could create structured enhancements in the electron density in the cusp/cleft region. *Moen et al.* [2002] found spatial structures in the electron density that mapped closely to the precipitation and proposed that the initial source of the decameter-scale HF backscatter targets may result from fine structure within the precipitation itself. Our results support this idea of a two-step process, which was originally suggested by *Kelley et al.* [1982]. When a flux tube drifts through a region of intense cusp aurora, structured particle precipitation can generate irregularities at kilometer scale, or even down to a few hundred meter scale. The life time of these irregularities depends on loss processes like how quickly the plasma can diffuse across the magnetic field. According to *Kelley* [2009, p. 472] the time scale for perpendicular diffusion is $\tau_D = (k^2 D_\perp)^{-1}$, where the wave number is $k = 2\pi/\lambda$, and the perpendicular diffusion coefficient $D_\perp$ has typical values of 10–50 $m^2\ s^{-1}$. ICI-2 was launched near solar minimum, so it is reasonable to assume the diffusion coefficient to be near its lower range [e.g., *Khocholava*, 1977]. It gives diffusion time scales of 70 h for 10 km structures, 42 min for 1 km structures, 10 min for 500 m structures, and 25 s for 100 m structures. Consequently, there is sufficient time for "seed" irregularities of a few hundred meters to survive a transit time of a few minutes, while the GD instability begin to break these irregularities down to decameter scales. The data presented in Figure 3e show that when conditions are optimal for growth of GD irregularities (e.g., 125–140 s after launch), the time scale can be as low as a few seconds (or a few tens of seconds). So in a couple of minutes there will be sufficient time for intense decameter GD irregularities to develop. This could also explain why the equatorward edge of the aurora and the HF backscatter always seem to be colocated in the cusp region.

4. Summary and Concluding Remarks

[25] We have presented in situ measurements from a sounding rocket and investigated fine-scale structures in polar cap patches and the growth of *F* region plasma irregularities in the cusp ionosphere. High-resolution sounding

rocket data from ICI-2 were combined with ground-based data; an all-sky camera, the EISCAT Svalbard Radar, and the SuperDARN Hankasalmi radar. These data sets allowed us to characterize the spatial structure of the observed *F* region irregularities and to derive instability growth rates at various spatial scales. Except for a promising interval of 4–6 km irregularities, the growth rate of the Kelvin-Helmholtz (KH) mechanism was too slow to explain any of the observed plasma irregularities, and we found the gradient drift (GD) mechanism to be dominating the production of the observed *F* region irregularities. We also noticed that the strongest plasma irregularities were observed only two minutes after a significant enhancement in the aurora (i.e., 125–140 s after launch). It leads us to propose a two-step irregularity generation process: (1) the structured particle precipitation generates weak "seed" irregularities at scales of kilometers to a few hundred meters, and (2) the GD instability will then break these "seed" irregularities very efficiently down into decameter scales.

[26] **Acknowledgments.** We thank the ACE MAG instrument team and the ACE Science Center for providing the ACE data. EISCAT is an international association supported by research organizations in Norway (NFR), Sweden (VR), Finland (SA), Japan (NIPR and STEL), China (CRIRP), the United Kingdom (STFC), Germany (DFG, till 2011), and France (CNRS, till 2005). We thank the SuperDARN PIs for provision of the radar data. SuperDARN operations at the University of Leicester are supported by the Radio and Space Plasma Physics group, and M.L. is funded by STFC grants PP/E000983/1 and ST/H002480/1. This project has also been sponsored by the Research Council of Norway, Andoya Rocket Range, COST action ES0803, and Air Force Office of Scientific Research, Air Force Material Command, USAF, under grant FA8655-10-1-3003.

[27] Robert Lysak thanks the reviewers for their assistance in evaluating this paper.

References

Baker, K. B., R. A. Greenwald, and R. T. Tsunoda (1983), Very high latitude *F* region irregularities observed by HF-radar backscatter, *Geophys. Res. Lett.*, *10*(9), 904–907, doi:10.1029/GL010i009p00904.

Baker, K. B., J. R. Dudeney, R. A. Greenwald, M. Pinnock, P. T. Newell, A. S. Rodger, N. Mattin, and C.-I. Meng (1995), HF radar signatures of the cusp and low-latitude boundary layer, *J. Geophys. Res.*, *100*(A5), 7671–7695, doi:10.1029/94JA01481.

Basu, S., S. Basu, E. MacKenzie, P. F. Fougere, W. R. Coley, N. C. Maynard, J. D. Winningham, M. Sugiura, W. B. Hanson, and W. R. Hoegy (1988), Simultaneous density and electric field fluctuation spectra associated with velocity shears in the auroral oval, *J. Geophys. Res.*, *93*(A1), 115–136, doi:10.1029/JA093iA01p00115.

Basu, S., S. Basu, E. MacKenzie, W. R. Coley, J. R. Sharber, and W. R. Hoegy (1990), Plasma structuring by the gradient drift instability at high latitudes and comparison with velocity shear driven processes, *J. Geophys. Res.*, *95*(A6), 7799–7818, doi:10.1029/JA095iA06p07799.

Basu, S., S. Basu, P. K. Chaturvedi, and C. M. Bryant Jr. (1994), Irregularity structures in the cusp/cleft and polar cap regions, *Radio Sci.*, *29*(1), 195–207, doi:10.1029/93RS01515.

Basu, S., E. J. Weber, T. W. Bullett, M. J. Keskinen, E. MacKenzie, P. Doherty, R. Sheehan, H. Kuenzler, P. Ning, and J. Bongiolatti (1998), Characteristics of plasma structuring in the cusp/cleft region at Svalbard, *Radio Sci.*, *33*(6), 1885–1899, doi:10.1029/98RS01597.

Bates, H. F. (1959), The height of *F*-layer irregularities in the Arctic ionosphere, *J. Geophys. Res.*, *64*(9), 1257–1265, doi:10.1029/JZ064i009p01257.

Bates, H. F., and P. R. Albee (1970), Aspect sensitivity of *F*-layer HF backscatter echoes, *J. Geophys. Res.*, *75*(1), 165–170, doi:10.1029/JA075i001p00165.

Bekkeng, T. A., K. S. Jacobsen, J. K. Bekkeng, A. Pedersen, T. Lindem, J.-P. Lebreton, and J. I. Moen (2010), Design of a multi-needle Langmuir probe system, *Meas. Sci. Technol.*, *21*, 085903, doi:10.1088/0957-0233/21/8/085903.

Buchau, J., B. W. Reinisch, E. J. Weber, and J. G. Moore (1983), Structure and dynamics of the winter polar cap *F* region, *Radio Sci.*, *18*(6), 995–1010, doi:10.1029/RS018i006p00995.

Carlson, H. C., T. Pedersen, S. Basu, M. Keskinen, and J. Moen (2007), Case for a new process, not mechanism, for cusp irregularity production, *J. Geophys. Res.*, *112*, A11304, doi:10.1029/2007JA012384.

Carlson, H. C., K. Oksavik, and J. Moen (2008), On a new process for cusp irregularity production, *Ann. Geophys.*, *26*, 2871–2885, doi:10.5194/angeo-26-2871-2008.

Cerisier, J. C., J. J. Berthelier, and C. Beghin (1985), Unstable density gradients in the high-latitude ionosphere, *Radio Sci.*, *20*(4), 755–761, doi:10.1029/RS020i004p00755.

Crowley, G. (1996), Critical review of ionospheric patches and blobs, in *Review of Radio Science 1993–1996*, edited by W. R. Stone, chapter 27, 619–648, Oxford Sci. Publ., Oxford, U. K.

Crowley, G., A. J. Ridley, D. Deist, S. Wing, D. J. Knipp, B. A. Emery, J. Foster, R. Heelis, M. Hairston, and B. W. Reinisch (2000), Transformation of high-latitude ionospheric *F* region patches into blobs during the March 21, 1990, storm, *J. Geophys. Res.*, *105*(A3), 5215–5230, doi:10.1029/1999JA900357.

D'Angelo, N., and R. W. Motley (1962), Electrostatic oscillations near the ion cyclotron frequency, *Phys. Fluids*, *5*, 633–634, doi:10.1063/1.1706672.

Dandekar, B. S. (2002), Solar cycle dependence of polar cap patch activity, *Radio Sci.*, *37*(1), 1013, doi:10.1029/2000RS002562.

Dyson, P. L. (1969), Direct measurements of the size and amplitude of irregularities in the topside ionosphere, *J. Geophys. Res.*, *74*(26), 6291–6303, doi:10.1029/JA074i026p06291.

Fejer, B. G., and M. C. Kelley (1980), Ionospheric irregularities, *Rev. Geophys.*, *18*(2), 401–454, doi:10.1029/RG018i002p00401.

Gondarenko, N. A., and P. N. Guzdar (2004), Plasma patch structuring by the nonlinear evolution of the gradient drift instability in the high-latitude ionosphere, *J. Geophys. Res.*, *109*, A09301, doi:10.1029/2004JA010504.

Hanuise, C. (1983), High-latitude ionospheric irregularities: A review of recent radar results, *Radio Sci.*, *18*(6), 1093–1121, doi:10.1029/RS018i006p01093.

Hanuise, C., J. P. Villain, and M. Crochet (1981), Spectral studies of *F* region irregularities in the auroral zone, *Geophys. Res. Lett.*, *8*(10), 1083–1086, doi:10.1029/GL008i010p01083.

Hanuise, C., J. P. Villain, C. Beghin, and G. Caudal (1985), Small-scale irregularities in the high-latitude *F* region, *AGARD Conf. Proc.*, *382*, 1–12.

Heelis, R. A., D. McEwen, and W. Guo (2002), Ion and neutral motions observed in the winter polar upper atmosphere, *J. Geophys. Res.*, *107*(A12), 1476, doi:10.1029/2002JA009359.

Hosokawa, K., S. Yamashita, P. Stauning, N. Sato, A. S. Yukimatu, and T. Iyemori (2004), Origin of the SuperDARN broad Doppler spectra: Simultaneous observation with Oersted satellite magnetometer, *Ann. Geophys.*, *22*, 159–168, doi:10.5194/angeo-22-159-2004.

Hudson, M. K., and M. C. Kelley (1976), The temperature gradient drift instability at the equatorward edge of the ionospheric plasma trough, *J. Geophys. Res.*, *81*(22), 3913–3918, doi:10.1029/JA081i022p03913.

Jacobsen, K. S., A. Pedersen, J. I. Moen, and T. A. Bekkeng (2010), A new Langmuir probe concept for rapid sampling of space plasma electron density, *Meas. Sci. Technol.*, *21*, 085902, doi:10.1088/0957-0233/21/8/085902.

Kelley, M. C. (2009), *The Earth's Ionosphere: Plasma Physics and Electrodynamics*, *International Geophysics Series*, vol. 96, Academic, San Diego, Calif.

Kelley, M. C., and P. M. Kintner (1978), Evidence for two-dimensional inertial turbulence in a cosmic-scale low-β plasma, *Astrophys. J.*, *220*, 339–345, doi:10.1086/155911.

Kelley, M. C., K. D. Baker, J. C. Ulwick, C. L. Rino, and M. J. Baron (1980), Simultaneous rocket probe, scintillation, and incoherent scatter radar observations of irregularities in the auroral zone ionosphere, *Radio Sci.*, *15*(3), 491–505, doi:10.1029/RS015i003p00491.

Kelley, M. C., J. F. Vickrey, C. W. Carlson, and R. Torbert (1982), On the origin and spatial extent of high-latitude *F* region irregularities, *J. Geophys. Res.*, *87*(A6), 4469–4475, doi:10.1029/JA087iA06p04469.

Keskinen, M. J., and S. L. Ossakow (1983), Theories of high-latitude ionospheric irregularities: A review, *Radio Sci.*, *18*(6), 1077–1091, doi:10.1029/RS018i006p01077.

Keskinen, M. J., H. G. Mitchell, J. A. Fedder, P. Satyanarayana, S. T. Zalesak, and J. D. Huba (1988), Nonlinear evolution of the Kelvin-Helmholtz instability in the high-latitude ionosphere, *J. Geophys. Res.*, *93*(A1), 137–152, doi:10.1029/JA093iA01p00137.

Khocholava, G. M. (1977), On diffusion-recombination parameters in the *F* region of the ionosphere, *J. Atmos. Terr. Phys.*, *39*, 389–391, doi:10.1016/S0021-9169(77)90154-4.

Kindel, J. M., and C. F. Kennel (1971), Topside current instabilities, *J. Geophys. Res.*, *76*(13), 3055–3078, doi:10.1029/JA076i013p03055.

Kintner, P., and N. D'Angelo (1977), A transverse Kelvin-Helmholtz instability in a magnetized plasma, *J. Geophys. Res.*, *82*(10), 1628–1630, doi:10.1029/JA082i010p01628.

Linson, L. M., and J. B. Workman (1970), Formation of striations in ionospheric plasma clouds, *J. Geophys. Res.*, *75*, 3211–3219, doi:10.1029/JA075i016p03211.

Lorentzen, D. A., N. Shumilov, and J. Moen (2004), Drifting airglow patches in relation to tail reconnection, *Geophys. Res. Lett.*, *31*, L02806, doi:10.1029/2003GL017785.

Lorentzen, D. A., J. Moen, K. Oksavik, F. Sigernes, Y. Saito, and M. G. Johnsen (2010), In situ measurements of a newly created polar cap patch, *J. Geophys. Res.*, *115*, A12323, doi:10.1029/2010JA015710.

McEwen, D. J., and D. P. Harris (1995), Observations of *F*-layer patches and their convection over the north magnetic pole, *Adv. Space Res.*, *16*(1), 69–72, doi:10.1016/0273-1177(95)00101-J.

McEwen, D. J., D. P. Harris, J. W. MacDougall, and I. F. Grant (1995), Drifting *F*-layer patches over the magnetic pole, *J. Geomagn. Geoelectr.*, *47*, 527–537, doi:10.5636/jgg.47.527.

McEwen, D. J., W. Guo, J. W. MacDougall, and P. T. Jayachandran (2004), The polar ionosphere, *Adv. Space Res.*, *34*(9), 2080–2084, doi:10.1016/j.asr.2004.06.011.

Milan, S. E., T. K. Yeoman, and M. Lester (1998), The dayside auroral zone as a hard target for coherent HF radars, *Geophys. Res. Lett.*, *25*(19), 3717–3720, doi:10.1029/98GL02781.

Milan, S. E., M. Lester, S. W. H. Cowley, J. Moen, P. E. Sandholt, and C. J. Owen (1999), Meridian-scanning photometer, coherent HF radar, and magnetometer observations of the cusp: A case study, *Ann. Geophys.*, *17*, 159–172, doi:10.1007/s00585-999-0159-5.

Moen, J., H. C. Carlson, S. E. Milan, N. Shumilov, B. Lybekk, P. E. Sandholt, and M. Lester (2000), On the collocation between dayside auroral activity and coherent HF radar backscatter, *Ann. Geophys.*, *18*, 1531–1549, doi:10.1007/s00585-001-1531-2.

Moen, J., I. K. Walker, L. Kersley, and S. E. Milan (2002), On the generation of cusp HF backscatter irregularities, *J. Geophys. Res.*, *107*(A4), 1044, doi:10.1029/2001JA000111.

Moen, J., N. Gulbrandsen, D. A. Lorentzen, and H. C. Carlson (2007), On the MLT distribution of *F* region polar cap patches at night, *Geophys. Res. Lett.*, *34*, L14113, doi:10.1029/2007GL029632.

Moen, J., K. Oksavik, T. Abe, M. Lester, Y. Saito, T. A. Bekkeng, and K. S. Jacobsen (2012), First in situ measurements of HF radar echoing targets, *Geophys. Res. Lett.*, *39*, L07104, doi:10.1029/2012GL051407.

Oksavik, K., F. Søraas, J. Moen, R. Pfaff, J. A. Davies, and M. Lester (2004), Simultaneous optical, CUTLASS HF radar, and FAST spacecraft observations: Signatures of boundary layer processes in the cusp, *Ann. Geophys.*, *22*, 511–525, doi:10.5194/angeo-22-511-2004.

Oksavik, K., V. L. Barth, J. Moen, and M. Lester (2010), On the entry and transit of high-density plasma across the polar cap, *J. Geophys. Res.*, *115*, A12308, doi:10.1029/2010JA015817.

Oksavik, K., J. I. Moen, E. H. Rekaa, H. C. Carlson, and M. Lester (2011), Reversed flow events in the cusp ionosphere detected by SuperDARN HF radars, *J. Geophys. Res.*, *116*, A12303, doi:10.1029/2011JA016788.

Ossakow, S. L., and P. K. Chaturvedi (1979), Current convective instability in the diffuse aurora, *Geophys. Res. Lett.*, *6*(4), 332–334, doi:10.1029/GL006i004p00332.

Ossakow, S. L., P. K. Chaturvedi, and J. B. Workman (1978), High-altitude limit of the gradient drift instability, *J. Geophys. Res.*, *83*(A6), 2691–2693, doi:10.1029/JA083iA06p02691.

Pedersen, T. R., B. G. Fejer, R. A. Doe, and E. J. Weber (2000), An incoherent scatter radar technique for determining two-dimensional horizontal ionization structure in polar cap *F* region patches, *J. Geophys. Res.*, *105*(A5), 10,637–10,655, doi:10.1029/1999JA000073.

Pryse, S. E., A. G. Wood, H. R. Middleton, I. W. McCrea, and M. Lester (2006), Reconfiguration of polar-cap plasma in the magnetic midnight sector, *Ann. Geophys.*, *24*, 2201–2208, doi:10.5194/angeo-24-2201-2006.

Reid, G. C. (1968), The formation of small-scale irregularities in the ionosphere, *J. Geophys. Res.*, *73*(5), 1627–1640, doi:10.1029/JA073i005p01627.

Rodger, A. S., and A. C. Graham (1996), Diurnal and seasonal occurrence of polar cap patches, *Ann. Geophys.*, *14*, 533–537, doi:10.1007/s00585-996-0533-5.

Rodger, A. S., M. Pinnock, J. R. Dudeney, K. B. Baker, and R. A. Greenwald (1994), A new mechanism for polar patch formation, *J. Geophys. Res.*, *99*(A4), 6425–6436, doi:10.1029/93JA01501.

Rodger, A. S., S. B. Mende, T. J. Rosenberg, and K. B. Baker (1995), Simultaneous optical and HF radar observations of the ionospheric cusp, *Geophys. Res. Lett.*, *22*(15), 2045–2048, doi:10.1029/95GL01797.

Sojka, J. J., M. V. Subramanium, L. Zhu, and R. W. Schunk (1998), Gradient drift instability growth rates from global-scale modeling of the polar ionosphere, *Radio Sci.*, *33*(6), 1915–1928, doi:10.1029/98RS02490.

Tsunoda, R. T. (1988), High-latitude *F* region irregularities: A review and synthesis, *Rev. Geophys.*, *26*(4), 719–760, doi:10.1029/RG026i004p00719.

Villain, J. P., C. Beghin, and C. Hanuise (1986), ARCAD3-SAFARI coordinated study of auroral and polar *F* region ionospheric irregularities, *Ann. Geophys.*, *4*, 61–68.

Walker, I. K., J. Moen, L. Kersley, and D. A. Lorentzen (1999), On the possible role of cusp/cleft precipitation in the formation of polar-cap patches, *Ann. Geophys.*, *17*, 1298–1305, doi:10.1007/s00585-999-1298-4.

Weaver, P. F. (1965), Backscatter echoes from field-aligned irregularities in the *F* region, *J. Geophys. Res.*, *70*(21), 5425–5432, doi:10.1029/JZ070i021p05425.

Weber, E. J., J. Buchau, J. G. Moore, J. R. Sharber, R. C. Livingston, J. D. Winningham, and B. W. Reinisch (1984), *F*-layer ionization patches in the polar cap, *J. Geophys. Res.*, *89*(A3), 1683–1694, doi:10.1029/JA089iA03p01683.

Wood, A. G., S. E. Pryse, and J. Moen (2009), Modulation of nightside polar patches by substorm activity, *Ann. Geophys.*, *27*, 3923–3932, doi:10.5194/angeo-27-3923-2009.

Yeoman, T. K., M. Lester, S. W. H. Cowley, S. E. Milan, J. Moen, and P. E. Sandholt (1997), Simultaneous observations of the cusp in optical, DMSP and HF radar data, *Geophys. Res. Lett.*, *24*(17), 2251–2254, doi:10.1029/97GL02072.